Geophysical Journal International

Geophys. J. Int. (2012) **189,** 331–342 doi: 10.1111/j.1365-246X.2012.05380.x

On the sensitivity of surface NMR in the presence of electrical conductivity anomalies

J.A. Lehmann-Horn, M. Hertrich, S.A. Greenhalgh and A.G. Green

Institute of Geophysics, ETH Zürich, Switzerland. E-mail: jochenl@aug.ig.erdw.ethz.ch

Accepted 2012 January 9. Received 2012 January 3; in original form 2011 March 18

SUMMARY

The surface-NMR tomography technique is based on the principles of electromagnetic induction and proton spin dynamics. Electromagnetic fields emitted by large surface current-driven loops are employed to locate and quantify groundwater reservoirs. The oscillating magnetic fields interact with proton spins of water molecules in the electrically conductive subsurface. To study the influence of changing subsurface electrical properties on the nuclear spin response, we consider the spin magnetization as a virtual magnetic dipole receiver. The numerical solutions for the electric and magnetic fields of the transmitter and the virtual receiver in 3-D heterogeneous ground are based on the finite-element method. We explicitly compute the frequency-domain electromagnetic sensitivities for separate spin magnetizations in a groundwater aquifer to study the distortion of the NMR response because of electrical heterogeneities in the medium. Analyses of entire pulse moment sequences yield the cumulative sensitivities to electrical conductivity and water-content variations in the subsurface. We illustrate the influence of conductivity on NMR responses using a limited number of models. From these models we found that electrical conductivity anomalies in the shallow subsurface ($<$50 m) having values $\geq$0.1 S m^{-1} and volumes with linear dimensions in the order of our loop size (i.e. edge length 100 m) can have a strong influence on the NMR response and ought to be taken into account in the inversion of surface-NMR data. The effect increases non-linearly with increased body size, increased conductivity contrast and decreased anomaly depth.

Key words: Electromagnetic theory; Magnetic and electrical properties; Hydrogeophysics.

1 INTRODUCTION

Surface nuclear magnetic resonance (NMR) tomography provides information on water locations and volumes in the earth's subsurface (Weichman *et al.* 2000; Hertrich 2008). Advances over the past few years have extended the commonly employed 1-D surface-NMR sounding approach in a homogeneous resistive earth (Legchenko & Valla 2002) and 1-D layered conducting media (Shushakov 1996; Hunter & Kepic 2005) to 2-D surface-NMR tomography of heterogeneous distributions of groundwater (Hertrich *et al.* 2009). Recently, we devised improved forward and inverse modelling algorithms for surface-NMR tomography to take account of a 3-D electrically conductive earth, surface topography and arbitrary loop shapes (Lehmann-Horn *et al.* 2011).

The use of loops placed at the surface of the object under investigation is a common practice in biomedical, spectroscopic and geophysical NMR applications (Chen & Hoult 1989; Levitt 2002). In medicine, small radio frequency coils are employed to probe and image small human or animal tissues and organs (Doty *et al.* 2007). It is well known that the physical properties of the sample (i.e. electrical conductivity) influence the signal-to-noise ratio of the device. A conductive body in the immediate vicinity of the coil acts as an extra impedance element (resistor) in the equivalent circuit and therefore introduces additional thermal noise. The effectiveness of the system can be improved by increasing the distance between the coil and the conductive body. The phenomenon is called the lift-off effect (Suits *et al.* 1998). In geophysical applications it is difficult to lift the loop away from the conductive ground because the surface coils have diameters of tens to hundreds of metres.

The processing and interpretation of surface-NMR tomography data, to reconstruct the water-content distribution of the subsurface, requires knowledge of the subsurface electrical conductivity distribution. In most previous treatments, the conductivity structure was assumed to be known from accompanying electrical/electromagnetic (EM) surveying (e.g. geoelectric, time-domain EM) or borehole measurements. Because the surface-NMR technique is based on the principles of EM induction and spin dynamics, the amplitude and phase of the NMR response carries information about the subsurface conductivity distribution. Braun *et al.* (2005) performed inversions of surface-NMR data (amplitude and phase information) to determine the water content distribution for a specified conductivity model. Later, they inverted NMR soundings directly for both electrical conductivity and water-content (Braun *et al.* 2008). But difficulties during the inversion process

may arise because of off-resonance effects which occur when the transmitter frequency is not exactly equal to the Larmor frequency (Walbrecker *et al.* 2011), and instrument phase changes associated with the generator, amplifier and matching network. Furthermore, post-processing steps applied to noise-contaminated data can seriously distort the NMR phases. Data recording and post-processing need to be done very carefully to avoid these effects. Moreover, surface-NMR sensitivity to electrical conductivity is a highly non-linear problem and until now has not been fully investigated. In this contribution, we present a new formulation for calculating the sensitivities explicitly, which could be incorporated into a non-linear inversion program to recover conductivity and water content simultaneously. Alternatively, if the conductivity structure is known from EM measurements, then the influence can be directly studied. Either way, our goal is to enhance understanding of surface NMR sensitivity to electrical conductivity in the subsurface.

To compute the sensitivity kernels or Fréchet derivatives, we make use of a numerical forward modelling algorithm that we recently developed for a 3-D heterogeneous earth having arbitrary surface topography (Lehmann-Horn *et al.* 2011). The algorithm is based on a secondary magnetic vector potential approach that combines a thin wire line integral technique (the Biot–Savart law) with a finite-element method. The primary potentials are obtained using a line-integral over the transmitter, which can be of arbitrary shape lying on an uneven surface topography. The singularity introduced by the current source can be circumvented in this way (Zhdanov 2009). The finite-element method offers a powerful means to obtain the numerical solution for the secondary EM field in inhomogeneous media having complicated internal boundaries (Jin 2002; Davidson 2005; Hand 2008). Edge-based finite elements are employed for solving the Helmholtz equation for the secondary magnetic vector potential on an unstructured grid (Rieben *et al.* 2005).

The structure of this paper is as follows. We first introduce the principal equations that govern EM induction in the earth and the evolution of spin magnetization. We then discuss the sensitivity problem for electrical conductivity and liquid water. The spin magnetization is viewed as a virtual magnetic dipole receiver and the sensitivities are computed for the resulting frequency-domain EM problem (Fig. 1). This allows us to investigate the influence of changing electrical rock properties on spin magnetization in the subsurface and NMR response. Finally, we give a detailed analysis of entire surface-NMR sounding curves for several subsurface models that provide the cumulative sensitivity to water content and electrical conductivity variations. The focus of the models is on 3-D conductivity anomalies, because in future field experiments we are interested in making surface-NMR measurements in the presence of electrically conductive features such as (i) salt plumes that contaminate freshwater aquifers (Wooding 1997), (ii) freshwater bearing palaeochannels that are confined by dipping clay layers (Auken *et al.* 2008) and (iii) Arctic sea ice ridges where NMR signals are likely to be heavily influenced by the salty sea water (Eiken *et al.* 1995).

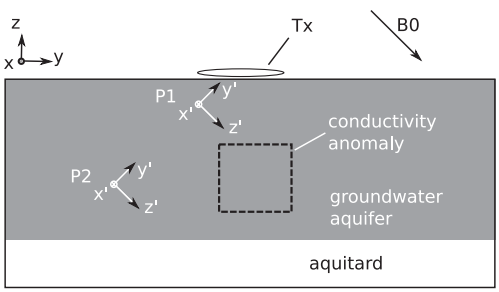

Figure 1. Schematic of the system used to study the distortion of electromagnetic fields generated by a transmitter (Tx) and virtual receivers (P1, P2) because of conductivity anomalies within a groundwater aquifer. The z-component of the Cartesian coordinate system (x, y, z, or geographic frame) is rotated in the direction of the static earth's magnetic field $\mathbf{B}_0$, having inclination 45° and declination 0° (x', y', z', or laboratory local coordinate frame).

2 THEORY

2.1 EM induction

Current-driven transmitter loops generate EM fields in the heterogeneous subsurface as well as in the air. Because we deal with a geophysical technique operating at a frequency ∼2 kHz, we can apply the quasi-static approximation and describe EM diffusion with Ampere's and Faraday's laws in the following form (Jackson 2006):

$$\nabla \times \mathbf{H} = \mathbf{J}_C + \mathbf{J}_E, \tag{1a}$$

$$\nabla \times \mathbf{E} = -\partial \mathbf{B}/\partial t + \mathbf{M}_S. \tag{1b}$$

The quantities $\mathbf{E}$ (V m^{-1}) and $\mathbf{H}$ (A m^{-1}) are the electric and magnetic field intensities, respectively. The quantity $\mathbf{J}_C = \sigma \cdot \mathbf{E}$ (A m^{-2}) is the electric conduction current density and $\mathbf{J}_E$ (A m^{-2}) is the external electric current density (i.e. electric source term). The magnetic current density $\mathbf{M}_S = -\mu_0 \partial \mathbf{M}/\partial t$ may either be related to a magnetic dipole (e.g. a small current loop) or a macroscopic spin magnetization $\mathbf{M}$ (A m^{-1}). The magnetic field intensity is associated with the magnetic flux density $\mathbf{B}$ (T = Vs m^{-2}) by $\mathbf{B} = \mu \mathbf{H}$. The electrical conductivity σ (S m^{-1}) and the magnetic permeability μ [Vs (Am)$^{-1}$] define the physical properties of the media. In the following, μ is set to the magnetic permeability of vacuum μ_0.

Recently, we introduced a numerical algorithm (Lehmann-Horn *et al.* 2011) to solve eqs (1a) and (1b). In Fig. 2, we present the magnetic field lines for four separate models from a wide range of situations investigated. Each model involves an embedded conductive block of conductivity σ_a and size V_a' within a uniform host rock of $\sigma = 0.01$ S m^{-1}. The anomalous body heavily distorts the magnetic field. The degree of distortion is dependent on the size and conductivity of the anomaly.

2.2 The evolution of the spin magnetization

In geophysical applications, it is common to use a geographical coordinate system (x, y, z; see Fig. 3a). For our sensitivity analysis, we introduce a rotated Cartesian coordinate system or laboratory frame (x', y', z'; see Fig. 3b). The new z'-axis coincides with the direction of the static earth's magnetic field $\mathbf{B}_0$.

The equilibrium spin magnetization M_0 (A m^{-1}) which is parallel to the static field is given by Curie's law (Chen & Hoult 1989):

$$M_0 = \frac{\hbar^2 \gamma^2 N}{4 k_B T} \mathbf{B}_0, \tag{2}$$

where $\hbar$ (Js) is the reduced Planck constant, the quantity γ (Ts^{-1}) is the gyromagnetic ratio for hydrogen, N is the number of protons in a unit volume (m^{-3}), k_B (J K^{-1}) is Boltzmann's constant, $\mathbf{B}_0$ is the strength of the static magnetic field and T is the absolute temperature (in K).

The dynamics of $\mathbf{M}$ (A m^{-1}) under the influence of an external magnetic field $\mathbf{B}_e$ (T) can be described classically by the Bloch

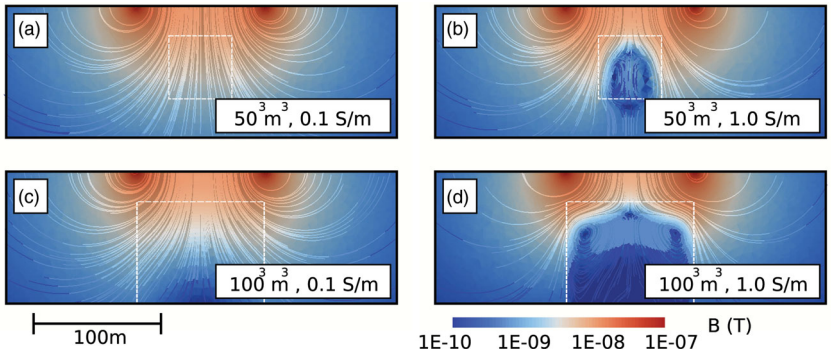

Figure 2. Magnetic field strength distribution in the subsurface generated by a loop of edge length $e = 100$ m in the presence of an electrically conductivity anomaly σ_a of volume V_a'. (a) $\sigma_a = 0.1$ S m^{-1}, $V_a' = 50^3$m^3, (b) $\sigma_a = 1.0$ S m^{-1}, $V_a' = 50^3$m^3, (c) $\sigma_a = 0.1$ S m^{-1}, $V_a' = 100^3$m^3 and (d) $\sigma_a = 1.0$ S m^{-1}, $V_a' = 100^3$m^3. The conductive body is located 25 m beneath the surface. Field lines are shown in the vertical plane that passes through the loop centre.

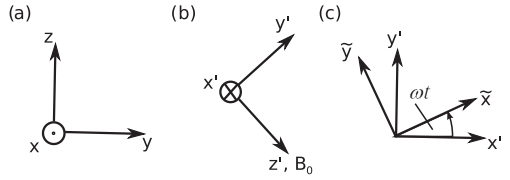

Figure 3. Coordinate systems: (a) geographical frame, (b) laboratory frame, z'-axis is parallel to static magnetic field $\mathbf{B}_0$ and (c) positively rotating frame. The latter is coincident with the laboratory frame at time $t = 0$.

equations (Bloch 1946):

$$\frac{\partial \mathbf{M}}{\partial t} = \gamma(\mathbf{M} \times \mathbf{B}_e) - \frac{M_{x'}}{T_2}\mathbf{x}' - \frac{M_{y'}}{T_2}\mathbf{y}' - \frac{M_{z'} - M_0}{T_1}\mathbf{z}'. \tag{3}$$

The quantities T_1 and T_2 are known as the longitudinal and transverse relaxation parameters, respectively. They depend on the rock and fluid properties of the porous medium. The external magnetic field $\mathbf{B}_e$ here comprises two parts, the alternating magnetic field $\mathbf{B}_1$ of the transmitter and the static earth's field $\mathbf{B}_0$:

$$\mathbf{B}_e = \mathbf{B}_1 + \mathbf{B}_0. \tag{4}$$

The transmitter operates at the Larmor frequency $\omega_L = -\gamma \mathbf{B}_0$ and the magnitude of $\mathbf{B}_1$ scales linearly with the strength of the input current. When the alternating magnetic field $\mathbf{B}_1$ is applied for a time period τ, the proton spin magnetization is tilted to a certain flip angle (into the x'- and y'-plane) and oscillates (precesses) around the z'-axis at frequency ω_L. The negative sign in the ω_L formula above indicates that the precession around $\mathbf{B}_0$ is a left-hand rotation. It is common practice to neglect the z'-component of the $\mathbf{B}_1$ field because $B_{1z'} \ll B_{0z'}$ (Levitt 2002). Following the approach of Hoult (2000), the magnetic field x'- and y'-components of the transmitter can be written in complex notation as:

$$B_{1x'} = IC_{x'}e^{i\alpha}, \tag{5a}$$

$$B_{1y'} = IC_{y'}e^{i\beta}. \tag{5b}$$

The parameters $C_{x'}$ and $C_{y'}$ are the position-, frequency- and loop size-dependent attenuation factors, and α and β are the phase changes produced by the conduction currents. For simplicity, the phase of the transmitter current I is set to zero.

The evolution of spin magnetization is treated in a reference frame ($\tilde{x}$, $\tilde{y}$, $\tilde{z}$; see Fig. 3c) that rotates around the z'-axis at frequency ω_L (denoted by tildes). The axes of the rotating frame are set to coincide with the laboratory frame at $t = 0$. Note that this rotating frame is common to all spins throughout the subsurface, independent of their location.

In Fig. 4, we present an illustrative example of the evolution of the three components of spin magnetization in the positively (denoted by(+)) rotating frame ($\tilde{M}_{x'}^{(+)}$, $\tilde{M}_{y'}^{(+)}$, $\tilde{M}_{z'}^{(+)}$). The pulse duration τ is set to 0.04 s. We distinguish between the excitation process (solid lines) and the relaxation process (dashed lines) of the spin experiment as a function of time for two different excitation fields. In the first case of a (real) magnetic field $B_{1x'} = 360$ nT without phase shift $\alpha = 0$ (non-conductive ground, black lines), the spin magnetization contains only $\tilde{y}$- and $\tilde{z}$-components. In the second case of an attenuated transmitter magnetic field $B_{1x'} = 200 + i50$ nT with phase shift $\alpha \neq 0$ (conductive ground, grey lines), the spin magnetization contains also an $\tilde{x}$-component. Moreover, there is a change in the $\tilde{M}_{z'}^{(+)}$ component compared to the first case. In the general case,

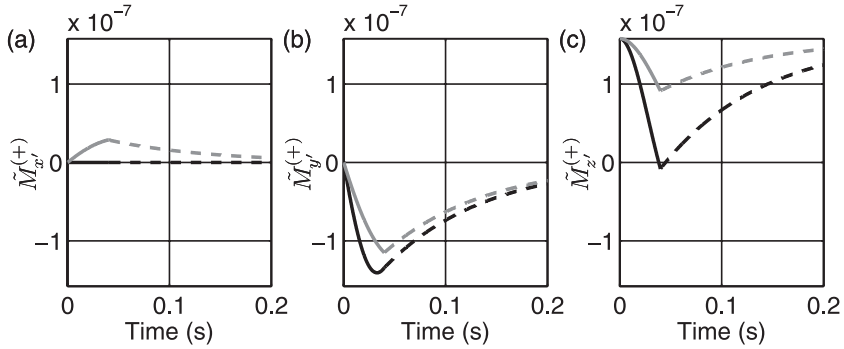

Figure 4. Evolution of spin magnetization $\tilde{M}^{(+)}$ in the positively rotating frame: excitation (solid lines) and relaxation process (dashed lines) because of an external magnetic field without a phase shift $\alpha = 0$ (black) and with phase shift $\alpha \neq 0$ (grey) based on a constant pulse duration of $\tau = 0.04$ s. The phase shift arises as a result of conductive structures.

the loop magnetic fields will exhibit spatial variations in direction, magnitude and phase throughout the subsurface (Fig. 2).

3 SENSITIVITY FORMULATION

3.1 A virtual receiver

Although the NMR method is directly sensitive to hydrogen protons, the electrical conductivity of the earth affects the behaviour of the transmitted and received EM fields. Several EM methods are routinely used in marine or land-based surveys to determine the electrical conductivity distribution in the subsurface (Nabighian 1992). Inverse theory techniques are required to extract this information from the observed data (Tarantola 2004). A major component of any non-linear local search inversion scheme is the ability to compute the sensitivities or Fréchet derivatives to update the medium parameters at each iteration. The sensitivities describe the perturbations in the measured quantity to perturbations in the model parameters. McGillivray & Oldenburg (1990) present a review of commonly used methods for sensitivity calculations. In a later paper, McGillivray & Oldenburg (1994) give a simple derivation of the Fréchet derivatives for the frequency-domain EM problem. Their approach exploits the principle of reciprocity, whereby the sensitivity of a receiver can be computed by assuming the receiver to be an adjoint source.

Starting from our eqs (1a) and (1b), they consider the primal problem for specified source distributions as well as an auxiliary problem (denoted by the overbars on the quantities) for a different electric and magnetic source specification. The primal problem is used to describe the EM field of the surface transmitter, whereas the auxiliary problem describes the receiver field. The combination permits one to derive the sensitivity of the receiver to electrical conductivity. Each boundary-value problem can be solved once the conditions appropriate to the source terms are specified on the boundary. The main result from McGillivray & Oldenburg (1994) can be written as:

$$\int_D \left(\bar{\mathbf{M}}_S \cdot \frac{\partial \mathbf{H}}{\partial \sigma_k} + \bar{\mathbf{J}}_E \cdot \frac{\partial \mathbf{E}}{\partial \sigma_k} \right) \mathrm{d}^3\mathbf{r}' = \int_D \bar{\mathbf{E}} \cdot \mathbf{E} \psi_k \mathrm{d}^3\mathbf{r}', \tag{6}$$

where $\bar{\mathbf{M}}_S$ (V m^{-2}) and $\bar{\mathbf{J}}_E$ (A m^{-2}) are the externally imposed magnetic and electric sources, for the auxiliary problem. The quantity $\bar{\mathbf{E}}$ is the electric field intensity given by the auxiliary Helmholtz equation, whereas $\mathbf{E}$ and $\mathbf{H}$ represent the electric and magnetic field intensities for the primal problem. The subsurface can be represented by L cells each of constant conductivity. Each cell D is a finite volume of discrete conductivity σ_k. The conductivity distribution is then determined by the function:

$$\sigma = \sum_{k=1}^{L} \sigma_k \psi_k, \tag{7}$$

where ψ_k is the boxcar function (i.e. $\psi_k = 1$ in cell k, zero elsewhere). The derivatives $\partial\mathbf{H}/\partial\sigma_k$ and $\partial\mathbf{E}/\partial\sigma_k$ in the integrand of eq. (6) are the sensitivities of the magnetic and electric fields to conductivity variations in region k. Eq. (6) shows that they are obtained by appropriately specifying the sources for the auxiliary fields and by integrating the dot product of the primal and auxiliary electric fields over the region in which ψ_k is non-zero. To compute the (electrical) sensitivities for a given subsurface receiver position (e.g. P1 and P2 in Fig. 1) requires solutions of eqs (1a) and (1b) for the electric field intensity $\mathbf{E}$ generated by the current in the transmitter loop $\mathbf{J}_E$ and the auxiliary field $\bar{\mathbf{E}}$ generated by the receiver, or adjoint source $\bar{\mathbf{M}}_S$. Obviously, we do not consider real or actual subsurface receivers. In what follows, they will be referred to as virtual receivers.

Because only magnetic fields perpendicular to $\mathbf{B}_0$ influence the evolution of spin magnetization, we only consider components perpendicular to the z'-direction. For a virtual magnetic receiver in the x'-direction, $\bar{\mathbf{M}}_S = \delta(\mathbf{r}' - \mathbf{r})\mathbf{x}'$ and setting $\bar{\mathbf{J}}_E = 0$, the sensitivity terms $\partial\mathbf{H}/\partial\sigma_k$ in eq. (6) simplify to:

$$\frac{\partial H_{x'}}{\partial \sigma_k} = \int_D \bar{\mathbf{E}} \cdot \mathbf{E} \psi_k \mathrm{d}^3\mathbf{r}'. \tag{8}$$

Similarly, we obtain for $\bar{\mathbf{M}}_S = \delta(\mathbf{r}' - \mathbf{r})\mathbf{y}'$ in the y'-direction:

$$\frac{\partial H_{y'}}{\partial \sigma_k} = \int_D \bar{\mathbf{E}} \cdot \mathbf{E} \psi_k \mathrm{d}^3\mathbf{r}'. \tag{9}$$

For the given virtual receiver positions P1 and P2 and directions x' andy', the sensitivities $\partial H_{x'}/\partial\sigma_k$ and $\partial H_{y'}/\partial\sigma_k$ are displayed in Fig. 5. The conductivity of the ground is assumed to be constant ($\sigma = 0.01$ S m^{-1}). If there was a conductive anomaly present in the blue region (negative sensitivity) of Fig. 5(d), then the magnetic field at position P2 would have decreased. In contrast, a conductivity anomaly in the red area (positive sensitivity) would result in a magnetic field increase at the virtual receiver position P2.

In surface-NMR measurements, one deals with hydrogen protons in water (ensemble of spins –1/2; Levitt 2002) that can be considered as virtual magnetic receivers distributed throughout the subsurface. Because we are interested in the sensitivity of the magnetic field rather than the magnetic field intensity, we rewrite eqs (8) and (9) in terms of $\partial B_{x'}/\partial\sigma_k$ and $\partial B_{y'}/\partial\sigma_k$ by multiplying with μ_0. Moreover, the auxiliary field $\bar{\mathbf{E}}$ in eqs (8) and (9) has to be computed for the spin magnetization vector after the pulse has been switched off.

3.2 NMR voltage strength calculation

The voltage signal induced in the receiver loop (here, the receiver coincides with the transmitter) by a spin magnetization in the subsurface (at position $\mathbf{r}$), after normalizing for the number of turns, is given by [Hoult 2000, p. 184, eq. (27)]:

$$K = 2\omega_L \tilde{\mathcal{M}}^{(+)} \hat{\mathcal{B}}_1^{(-)*}. \tag{10}$$

This function K is the product of (i) $\tilde{\mathcal{M}}^{(+)}$, the complex magnetization for the positively (+) rotating frame (denoted by tildes) and (ii) $\hat{\mathcal{B}}_1^{(-)*}$, the complex conjugate (denoted by a star) of the receiver magnetic field in the negatively (–) rotating frame at unit current (denoted by circumflex). An Argand diagram in which real numbers are defined along the $\tilde{x}$-axis and imaginary numbers along the $\tilde{y}$-axis is used to simplify the mathematics. The spin magnetization $\tilde{\mathcal{M}}^{(+)}$ is a function of the transmitter current I which generates the magnetic field $\tilde{\mathcal{B}}_1^{(+)}$ and the pulse duration τ (see Section 2.2). The product of current strength and pulse duration is defined as the pulse moment $q = I \cdot \tau$. Therefore, the voltage K is a function of position and pulse moment $K = K(q, \mathbf{r})$. The various quantities appearing in eq. (10) are defined as follows:

$$\tilde{\mathcal{B}}_1^{(-)} = \frac{1}{2}(B_{1x'} - i\,B_{1y'})^*, \tag{11}$$

$$\tilde{\mathcal{M}}^{(+)} = \tilde{M}_{x'}^{(+)} + i\,\tilde{M}_{y'}^{(+)} \tag{12}$$

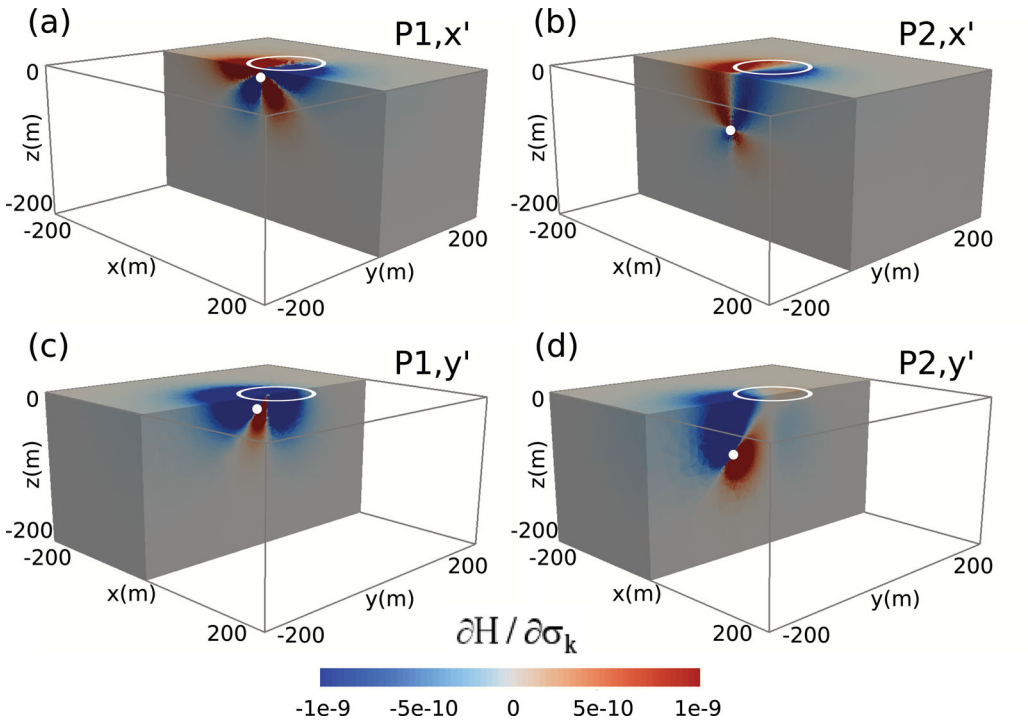

Figure 5. Electromagnetic sensitivity function $\partial H/\partial\sigma_k$ computed for two virtual receiver positions (white dots) P1 close to the surface in the (a) x'-direction, (c) y'-direction and P2 at depth in the (b) x'-direction, (d) y'-direction for a transmitter loop (white circle) with radius $r = 50$ m (see Fig. 1 for locations).

and ω_L was given earlier as the Larmor frequency. The components of magnetization $\tilde{M}^{(+)}_{x'}$ and $\tilde{M}^{(+)}_{y'}$ are a solution of the Bloch eq. (3) in the positive rotating frame after pulse extinction. The function K is well known as the kernel function or NMR sensitivity function to water. In the following, we are interested in the NMR sensitivity to electrical conductivity.

3.3 Sensitivity to electrical conductivity

Of special interest is the function $\partial K/\partial\sigma$ of the induced NMR voltage to variations in electrical conductivity (see eq. (10)). It is given by:

$$\frac{\partial K}{\partial\sigma} = 2\omega_L \left\{ \frac{\partial\tilde{\mathcal{M}}^{(+)}}{\partial\sigma}\hat{\mathcal{B}}_1^{(-)*} + \tilde{\mathcal{M}}^{(+)}\frac{\partial\hat{\mathcal{B}}_1^{(-)*}}{\partial\sigma} \right\}. \tag{13}$$

Because we aim to find a closed form solution for the sensitivity formulation and to simplify the mathematics, we consider the solution of the Bloch eq. (3) in the positive rotating frame by neglecting the relaxation terms [which is a common approximation in NMR applications (Weichman *et al.* 2000)] and assuming small flip angles [which is strictly only valid for small pulse moments or large distances to the coil (Hoult 2000)]

$$\tilde{\mathcal{M}}^{(+)} \approx -i\gamma\tau M_0\tilde{\mathcal{B}}_1^{(+)}, \tag{14}$$

$$\tilde{\mathcal{B}}_1^{(+)} = \frac{1}{2}(B_{1x'} + iB_{1y'}). \tag{15}$$

Substituting eqs (14) and (15) into eq. (13) gives:

$$\frac{\partial K}{\partial\sigma} \approx -i\gamma\tau M_0\omega_L I \left\{ \left(\frac{\partial\hat{B}_{1x'}}{\partial\sigma} + i\frac{\partial\hat{B}_{1y'}}{\partial\sigma} \right)\cdot\hat{\mathcal{B}}_1^{(-)*} + \left(\frac{\partial\hat{B}_{1x'}}{\partial\sigma} - i\frac{\partial\hat{B}_{1y'}}{\partial\sigma} \right)\cdot\hat{\mathcal{B}}_1^{(+)} \right\} \tag{16}$$

We introduce the abbreviation:

$$G = \frac{\partial\hat{B}_{1x'}}{\partial\sigma} + i\frac{\partial\hat{B}_{1y'}}{\partial\sigma}, \tag{17}$$

and finally obtain:

$$\frac{\partial K}{\partial\sigma} \approx -i\gamma\tau M_0\omega_L I \left\{ G\cdot\hat{\mathcal{B}}_1^{(-)*} + \hat{\mathcal{B}}_1^{(+)}\cdot G^* \right\}. \tag{18}$$

This expression is the sensitivity of the induced NMR voltage signal to electrical conductivity variations. In Appendix, two special cases ($B_{1x'} = 0$ and $B_{1y'} = 0$) that result in simplified versions of eq. (18) are considered.

3.4 Entire surface NMR response

The total surface-NMR signal sensed by the surface receiver loop is obtained by integrating the product of the water content distribution $f(\mathbf{r})$ and the spatially dependent function K [eq. (10)] over the entire volume:

$$V(q) = \int_V f(\mathbf{r})\cdot K(q,\mathbf{r})\mathrm{d}^3\mathbf{r}. \tag{19}$$

In Fig. 6, the surface-NMR sensitivities and sounding curve are demonstrated for a homogeneous conductivity model $\sigma = 0.01$ S m^{-1} (our reference model). Different regions in the subsurface are illuminated by varying the pulse moment q (see Figs 6a–c). Integrating the function K over the entire volume yields the surface-NMR sounding curve given in Fig. 6(d). The curve actually consists of two parts: a real part (shown by circles) and an imaginary part (shown by crosses). The curve appears smooth over the entire pulse moment sequence. Equally, it could be plotted as amplitude and phase.

By contrast, we show in Fig. 7 the equivalent computations for a model including a large anomaly (block of side length 100 m) at

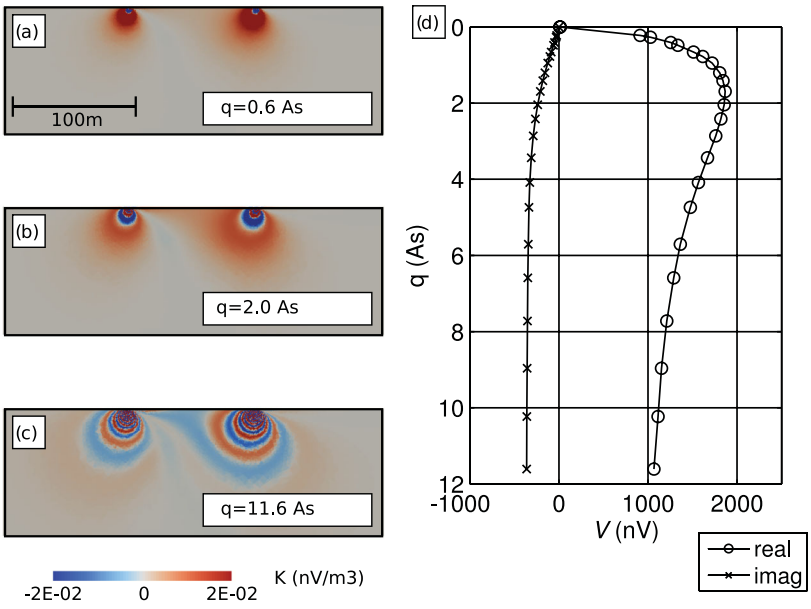

Figure 6. Surface-NMR sensitivities K (cross sections) of a homogeneous conductivity model ($\sigma = 0.01$ S m^{-1}; reference model) for pulse moments (a) $q = 0.6$ As, (b) $q = 2.0$ As and (c) $q = 11.6$ As. (d) Sounding curve for a homogeneous 100 m thick and 25 per cent water-saturated groundwater aquifer.

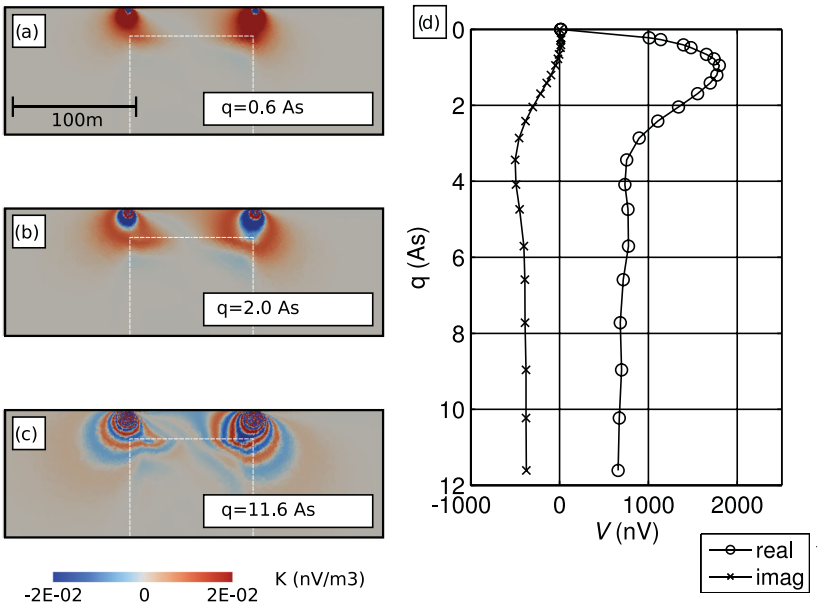

Figure 7. Same as Fig. 6, but including a conductivity anomaly of $\sigma_a = 1.0$ S m^{-1} and volume $V_a' = 100^3$ m^3 (shown by white boxes). See Fig. 2(d) for the equivalent magnetic field distribution.

25 m depth with a high conductivity $\sigma = 1$ S m^{-1} that disturbs the functions K (Figs 7a–c) and therefore the sounding curve (Fig. 7d). The function K is based on the EM field distribution shown in Fig. 2(d). Note the difference in the sounding curves in Figs 6(d) and 7(d). The perturbation in electrical conductivity results in a highly non-linear response in the surface-NMR voltage signal.

The entire sensitivity of the surface-NMR response to electrical conductivity can be obtained by differentiating eq. (19) to give:

$$\partial V/\partial\sigma = \int_V f(\mathbf{r}) \cdot \partial K/\partial\sigma \, \mathrm{d}^3\mathbf{r}. \tag{20}$$

The computation of eq. (19) is very expensive, because for each subsurface cell D a frequency-domain sensitivity problem has to be solved [see eqs (8) and (9)]. To perform a non-linear inversion in terms of electrical conductivity and water-content is even more expensive, because in each iteration of the optimization process all auxiliary problems have to be solved. The problem could be tackled on high-performance parallel computers, but at the present time would be very time consuming on a single workstation. However, the sensitivity formulation presented in eq. (18) is easily computed and allows one to estimate the influence of electrical conductivity anomalies on the NMR response.

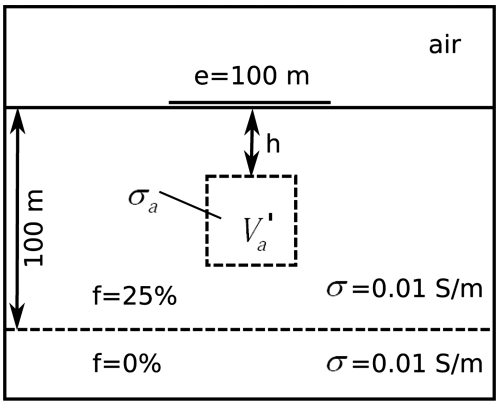

Figure 8. Synthetic 3-D anomaly model having a conductivity σ_a and a volume V_a' located at depth h in a background conductivity $\sigma = 0.01$ S m^{-1}. The loop edge length is $e = 100$ m. The aquifer has a thickness of 100 m and a water content of $f = 25$ per cent, whereas the aquitard has $f = 0$ per cent of water.

4 SYNTHETIC MODEL RESULTS

4.1 Applications

Details on the practical aspects of NMR surveying are beyond the scope of this paper and may be found, for example, in Hertrich *et al.* (2007) and Hertrich (2008). In this section, we first briefly identify and describe the types of hydrogeophysical example we are going to simulate, restricting the range of model parameters to those of practical relevance. The examples are illustrative only. They are intended to show the influence of conductivity structure on the NMR response. The loop shapes most commonly employed in surface NMR are circular or rectangular and vary from small loops of edge length (rectangular) or diameter (circular) $e = 10$ m up to $e = 100$ m. Here, we restrict our discussion to a rectangular loop of $e = 100$ m.

Most earth materials of hydrogeological interest have conductivities in the range of $\sigma = 0.001$ S m^{-1} (e.g. resistive basement) to $\sigma = 3.0$ S m^{-1} (e.g. saltwater intrusions). The thickness and size of an electrical conductor can vary from a few tens of metres (e.g. landfills) to hundred of metres (e.g. clay lens) and kilometres (e.g. saltwater intrusions). The conductor may be situated anywhere in the subsurface [several metres below the earth's surface (e.g. saltwater intrusion near the coast) down to several hundred metres]. A target for freshwater exploration is palaeochannels that are often bounded by conductive clay layers.

4.2 A conductive three-dimensional body

In the following examples, we consider the conductor as a saltwater intrusion into a freshwater aquifer (see Fig. 8 for model description). This is a commonly encountered situation (Wooding 1997). A rectangular loop is situated directly above a uniformly water-saturated groundwater layer $f = 25$ per cent that is 100 m thick and incorporates a 3-D electrical conductivity anomaly (conductivity σ_a and volume V_a'). The background conductivity σ is 0.01 S m^{-1}. The transmitter operates at a frequency $f = 2$ kHz and is situated in the earth's magnetic field, having inclination 45° and declination 0°.

Figs 9 and 10 show the computed surface-NMR response voltages $V(q)$ integrated across the entire probed volume for suites of pulse moments (sounding curves) for coincident transmitter–receiver configurations. The upper rows (a, b, c) show the real parts and the lower rows (d, e, f) the imaginary parts. The different figures correspond to conductive blocks at different depths below the surface and various block volumes are considered in each case.

In Fig. 9 the NMR responses are distorted by an anomaly of $\sigma_a = 0.1$ S m^{-1}, whereas in Fig. 10, the conductivity anomaly is

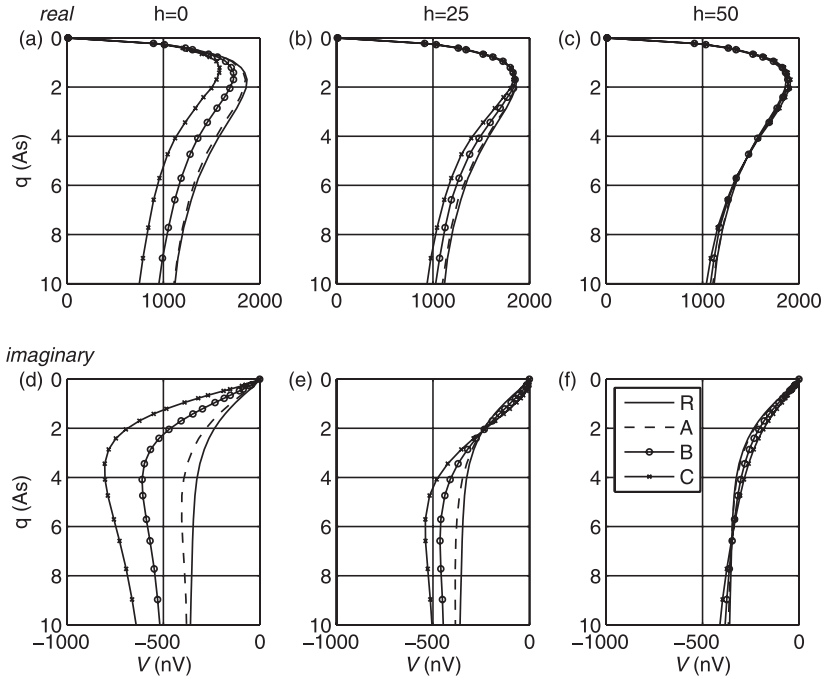

Figure 9. Surface-NMR sounding curves (complex voltage V versus pulse moment q) distorted by a conductive block of various anomaly volumes V_a'. Conductivity model: background conductivity ($\sigma = 0.01$ S m^{-1}) and anomalous block ($\sigma_a = 0.1$ S m^{-1}) that is situated at (a, d) $h = 0$ m, (b, e) $h = 25$ m and (c, f) $h = 50$ m below the surface (see Fig. 8 for model description); (a, b, c) real parts and (d, e, f) imaginary parts of sounding curves, each for volumes (R) $V_a' = 0$ (reference), (A) $V_a' = 50^3$ m^3, (B) $V_a' = 80^3$ m^3 and (C) $V_a' = 100^3$ m^3.

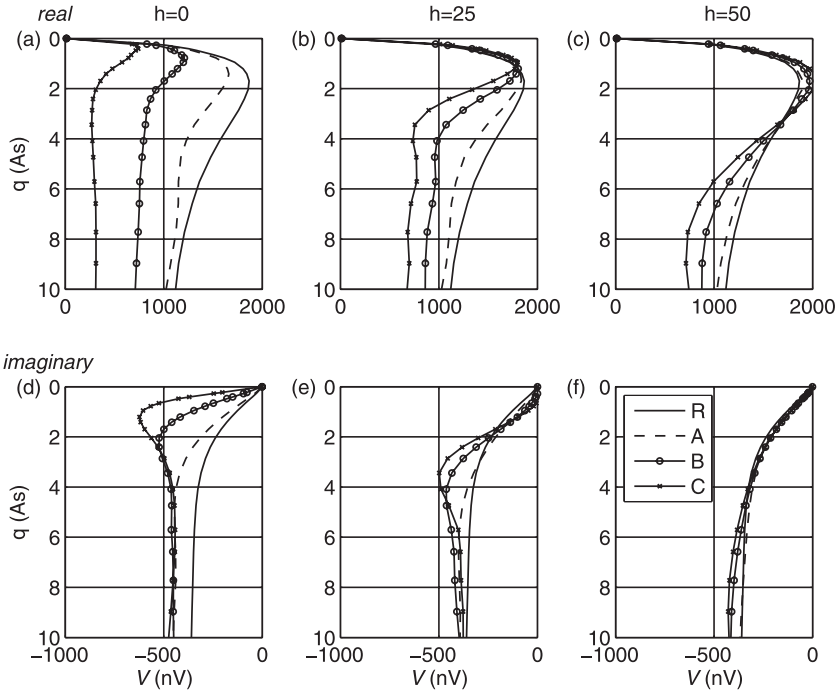

Figure 10. Same as Fig. 9, but for a higher anomalous conductivity $\sigma_a = 1.0$ S m^{-1}.

increased to $\sigma_a = 1.0$ S m^{-1}. In diagrams (a) and (d) of Figs 9 and 10, the tops of the anomalies are situated at the earth's surface $h = 0$ m. In diagrams (b) and (e), the tops of the bodies are at $h = 25$ m, whereas in diagrams (c) and (f) they are located at $h = 50$ m.

Sounding curve R is our reference curve (homogeneous conductive half-space), whereas curves A, B and C are for bodies having volumes $V_a' = 50^3\text{m}^3$, $V_a' = 80^3\text{m}^3$ and $V_a' = 100^3\text{m}^3$, respectively.

For a deep-seated ($h = 50$ m), small ($V_a' = 50^3\text{m}^3$) anomalous block with low conductivity ($\sigma_a = 0.1$ S m^{-1}) (Figs 9c and f), we observe very small derivations in the sounding curve relative to the reference curve. The derivations lie within the range of common noise levels (20–100 nV). Although larger volumes have a stronger influence on the response, they would be hard to distinguish under high noise conditions.

For an intermediate depth ($h = 25$ m) small body ($V_a' = 50^3\text{m}^3$) and a small contrast ($\sigma_a = 0.1$ S m^{-1}) (Figs 9b and e), we again observe only small derivations in the NMR response. Increasing the volume (curves B and C) has a significant influence on the curves. Differences up to 300 nV occur compared to the reference curve.

For the small, low volume body at shallow depth $h = 0$ m, $V_a' = 50^3\text{m}^3$ and $\sigma_a = 0.1$ S m^{-1} (Figs 9a and d), we find again relatively small fluctuations in the NMR response, but larger bodies ($V_a' = 80^3\text{m}^3$ or $V_a' = 100^3\text{m}^3$) have a significant influence on the curves. Voltage differences rise up to 500 nV.

Highly conductive bodies change the characteristics of the sounding curves. This is highlighted in Fig. 10. For $h = 50$ m, $V_a' = 50^3\text{m}^3$ and $\sigma_a = 1.0$ S m^{-1} (Figs 10c and f), we observe fluctuations in the sounding curve that lie in the range of common noise levels. But, compared to Fig. 9, increasing the volumes of the block has a stronger influence. Real parts are heavily affected by the anomaly at high pulse moments (5–10 As).

For $h = 25$ m, $V_a' = 50^3$ m^3 and $\sigma_a = 1.0$ S m^{-1} (Figs 10b and e), we obtain a slightly distorted sounding curve. Increasing the volume to 80^3 m^3 and 100^3m^3 has a strong effect on the signal. Real and imaginary parts are disturbed, especially at pulse moments 2–4 As.

For $h = 0$ m, $V_a' = 50^3\text{m}^3$ and $\sigma_a = 1.0$ S m^{-1} (Figs 10a and d), we observe significant influences on the NMR response. Increasing the anomalous body results in a severely perturbed curve compared to the reference, with differences of $\geq$1000 nV.

Fig. 11 shows the surface-NMR electrical sensitivity $\mathrm{d}V/\mathrm{d}\sigma$ plots as a function of pulse moment corresponding to the model B ($V_a' = 80^3\text{m}^3$) for which the NMR responses are shown in Figs 9 and 10. This function $\mathrm{d}V/\mathrm{d}\sigma$ is computed by the simple difference formula $\mathrm{d}V/\mathrm{d}\sigma = (V_2 - V_1)/(\sigma_2 - \sigma_1)$, where the indices indicate the model: (1) $\sigma_a = 0.1$ S m^{-1} and (2) $\sigma_a = 1.0$ S m^{-1}. The upper rows (a, b, c) show the real parts of the NMR sensitivity function and the lower rows (d, e, f) the imaginary parts. The three different diagrams in each row correspond to conductive blocks at different depths below the surface ($h = 0$ m, 25 m, 50 m). For most pulse moments ($q > 3.5$ As) the real part is negative, implying that an increase in electrical conductivity reduces the real part of the NMR signal (and conversely a decrease in conductivity increases the NMR signal). For small pulse moments, the real part of the voltage is positive (see Figs 11b and c). In contrast, the imaginary part shows a pronounced change of sign of the sensitivity with respect to the location of the anomalous body.

In general, we can make the following observation: the deeper the body, the higher the pulse moment values that show the disturbance in the sounding curves (see e.g. Figs 10d and e). Similarly, the deeper the body, the higher the pulse moment at which the minimum (real part) and maximum (imaginary part) in the electrical sensitivity function $\mathrm{d}V/\mathrm{d}\sigma$ occurs (see Fig. 11). The reason is that higher pulse moments illuminate the deeper structures. Clearly, the strongest disturbances appear when the body is situated at shallow depth directly beneath the loop and the conductivity contrast is high.

If shallow ($h \leq 50$ m) electrically conductive anomalies ($\sigma_a \geq 0.1$ S m^{-1}) are not taken into account in the NMR modelling, then the inversion of such data would yield highly misleading information.

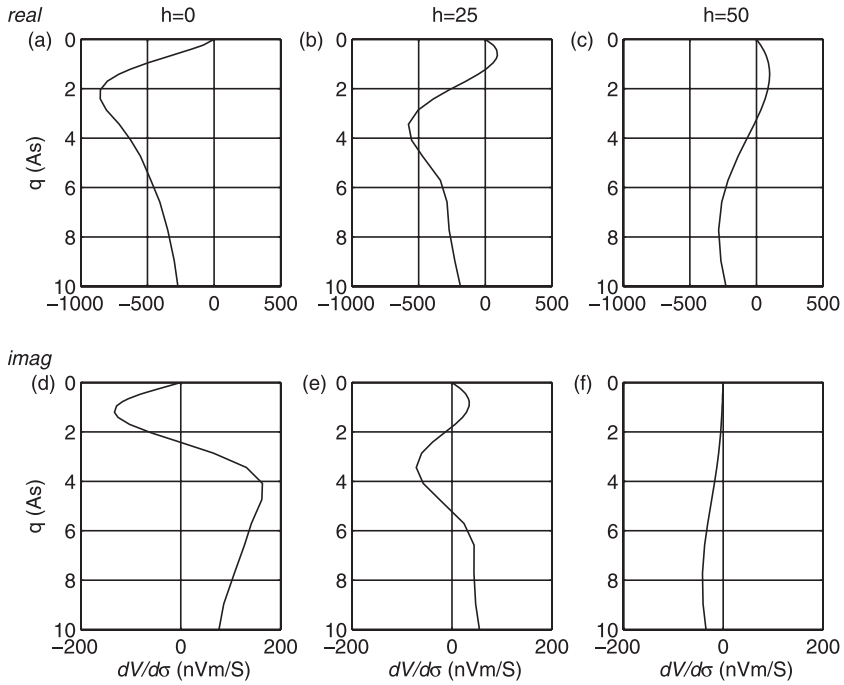

Figure 11. Surface-NMR (electrical) sensitivity function (complex voltage $\mathrm{d}V/\mathrm{d}\sigma$ versus pulse moment q) corresponding to the model B ($V_a' = 80^3$ m^3) in Figs 9 and 10. The function $\mathrm{d}V/\mathrm{d}\sigma$ is the difference between the two conductivity models $\mathrm{d}V/\mathrm{d}\sigma = (V_2 - V_1)/(\sigma_2 - \sigma_1)$ and determined by the indices: (1) $\sigma_a = 0.1$ S m^{-1} and (2) $\sigma_a = 1.0$ S m^{-1}. The different diagrams correspond to conductive blocks at different depths below the surface. The anomalous block is situated at (a, d) $h = 0$ m, (b, e) $h = 25$ m and (c, f) $h = 50$ m below the surface.

4.3 A dipping, conductive layer

Here, we investigate a common situation in hydrogeophysics that is known from time-domain EM measurements (Auken 2008) viz., a dipping conductive clay or saltwater layer underlying a freshwater aquifer (see Fig. 12). We want to investigate the influence of the conductive layer on the NMR response.

The layer dips at an angle of 20° (in the y-direction) and has a thickness of 75 m. Three NMR loops are situated along a profile in the y-direction. The position of the loop is defined by the quantity a, which takes on three separate values $a = -100$ m, $a = 0$ m and $a = 100$ m. The transmitters that operate at 2 kHz are situated in the local earth's magnetic field, which has an inclination of 45° and a declination of 0° (y-axis is directed towards North). The conductivity of the conductive layer is fixed at $\sigma = 1$ S m^{-1} for the following computations, but that of the overlying and underlying layers is allowed to vary. The water content in the aquifer is fixed at $f = 25$ per cent. In the conductive layer, the water content f is allowed to vary, whereas in the underlying basement the water content is set to $f = 0$ per cent for all computations.

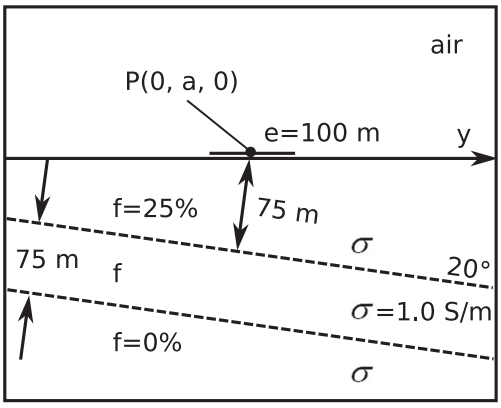

Figure 12. Synthetic dipping conductive layer model with variable water content f is situated in a varying background material σ and 75 m beneath the loop position $a = 0$ m (normal vector length of the dipping layer). The layer conductivity is fixed to 1 S m^{-1}. Loops (edge length $e = 100$ m) centre points P (0, a, 0) are varying along the y-axis.

In the first model (Fig. 13), the water content in the second layer (conductive layer) is $f = 25$ per cent. The computed sounding curves along the profile are shown for two different layer-conductivity models. The first set of curves (A) show the real and imaginary parts, respectively, for a moderate background conductivity of $\sigma = 0.01$ S m^{-1}. Following the profile from left to right ($a = -100$–100 m), we observe a significant difference between the sounding curves for high pulse moments. The difference appears because the water layer thickness increases from left to right. The imaginary parts are negative. The second set of curves (B) show the real and imaginary parts for a low background conductivity of $\sigma = 0.001$ S m^{-1}. The imaginary parts of the curves decrease compared to those of situation (A) and practically vanish for loop position $a = 100$ m.

In the second model (Fig. 14), we use the same conductivity parameters as described for Fig. 13, but change the water-content model. The water content of the second layer (conductive layer) is $f = 0$ per cent. We observe that the voltages are reduced because less water is available to contribute to the signal strength. Moreover, the imaginary part in the NMR response is reduced because water is absent in the conductive layer.

The first set of curves (A) show smaller imaginary parts. For the second set of curves (B), when the background material is more resistive, the imaginary parts change sign and are even smaller.

Figs 13 and 14 show the strong interaction between electrical conductivity and the water content. The NMR response is

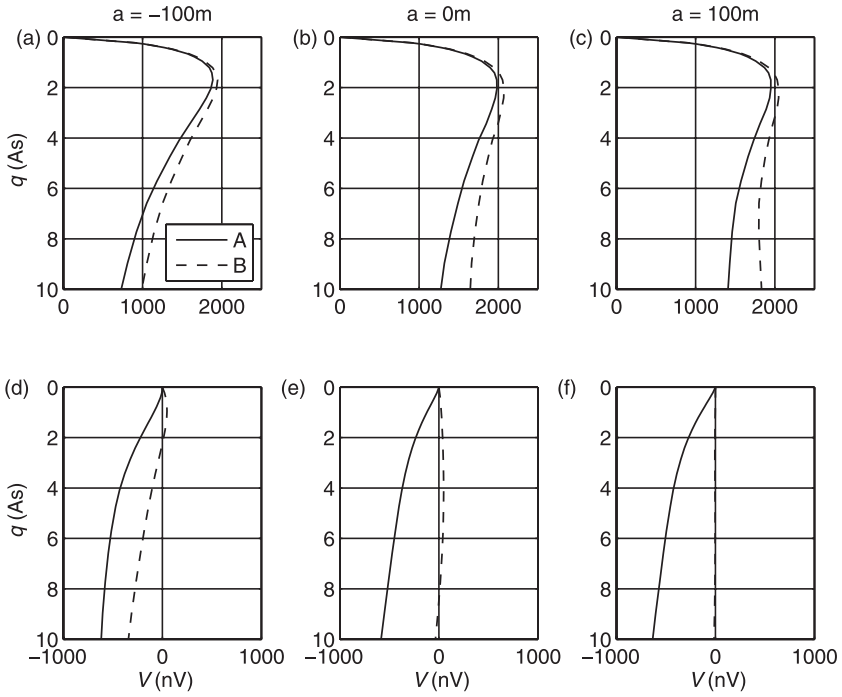

Figure 13. Surface-NMR sounding curves (complex voltage V versus pulse moment q) for a dipping conductive layer model as described in Fig. 12. Loops are located at (a, d) $a = -100$ m, (b, e) $a = 0$ m and (c, f) $a = 100$ m. Diagrams show (a, b, c) real parts and (d, e, f) imaginary parts for a layer conductivity (A) $\sigma = 0.01$ S m^{-1} and (B) $\sigma = 0.001$ S m^{-1}. Water content in conductive layer is $f = 25$ per cent.

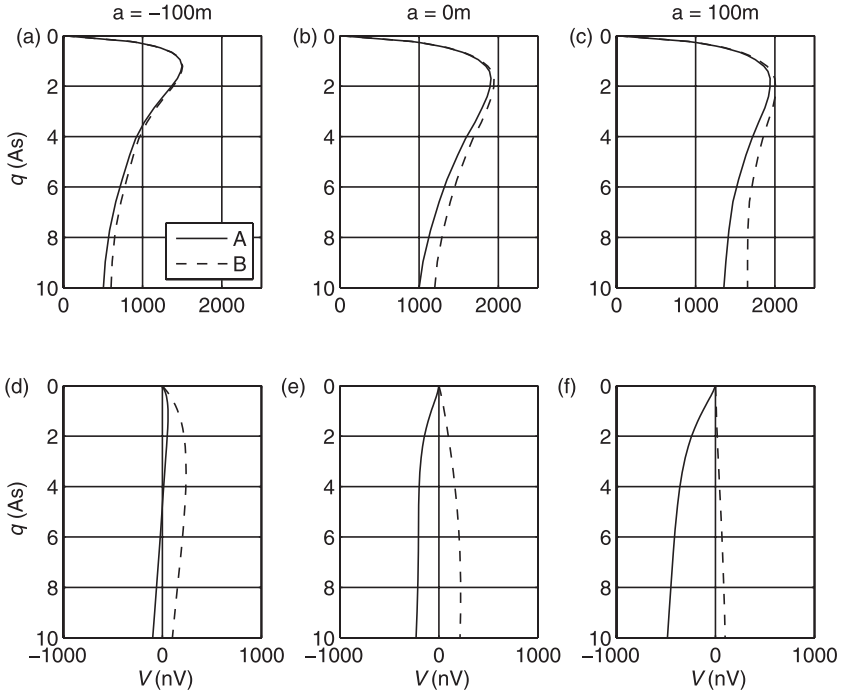

Figure 14. Same as Fig. 13, but water content in conductive layer $f = 0$ per cent. Layer conductivity (A) $\sigma = 0.01$ S m^{-1} and (B) $\sigma = 0.001$ S m^{-1}.

affected in a highly non-linear manner by the conductivity structure, but scales linearly with the water content. The effect of conductivity arises from both water-filled and dry conductive structures. The influence of the latter is smaller but nevertheless cannot be neglected. This is especially important for shallow conductors.

5 CONCLUSIONS

Surface-NMR tomography is directly sensitive to subsurface water. However, high electrical conductivities have a major influence on the impressed EM field distribution and thus affect the inverse problem. We have investigated the effects of 3-D electrical conductivity

anomalies on the NMR response. We employed a finite-element method and computed the NMR sensitivity in terms of electrical conductivity and water content. For the former, we assumed that the nuclear spin magnetization can be considered as a virtual magnetic dipole receiver. We gave a mathematical formulation for the NMR sensitivity to electrical conductivity. This was solved in the frequency-domain to study the influence of electrical conductivity on a single spin magnetization. By integrating the response across the entire water volume distribution model, we analysed entire sounding curves and illustrated the cumulative distortion of the measured NMR signal voltage. Conductivity anomalies (e.g. saltwater intrusions) in the order of 0.1–1 S m^{-1} had a significant influence on the NMR response, which was in the range of 100–1000 nV for 100 m loops and shallow-seated $\leq$50 bodies of similar dimension to the loop size. The influence was highly non-linear and depended on conductor size, position, depth and electrical conductivity contrast. The signal strength and phase shift were dependent on the presence and location of water. We have presented several synthetic models of hydrogeological relevance to illustrate these effects. A more complete investigation including loop size and scalability will be addressed in future studies. The derived NMR sensitivities to electrical conductivity could be incorporated in non-linear inversions to electrical conductivity and water content in the future.

ACKNOWLEDGMENTS

We wish to thank Jan Walbrecker and Thomas Kalscheuer from ETH Zurich for many helpful discussions on various aspects of NMR and electromagnetics. This research was supported by grants from the Swiss National Science Foundation and ETH Zurich.

REFERENCES

Auken, E., Christiansen, A.V., Jacobsen, L.H. & Sorensen, K.I., 2008. A resolution study of buried valleys using laterally constrained inversion of TEM data, *J. appl. Geophys.,* **65,** 12–20.

Bloch, F., 1946. Nuclear induction, *Phys. Rev.,* **70,** 460–474.

Braun, M., Hertrich, M. & Yaramanci, U., 2005. Study on complex inversion of magnetic resonance sounding signals, *Near Surf. Geophys.,* **3,** 155–163.

Braun, M. & Yaramanci U., 2008. Inversion of resistivity in magnetic resonance sounding, *J. appl. Geophys.,* **66,** 151–164.

Chen C.-N. & Hoult D.I., 1989. *Biomedical Magnetic Resonance Technology*, Adam Hilger, Bristol.

Davidson, D.B., 2005. *Computational Electromagnetics for RF and Microwave Engineering*, Cambridge University Press, Cambridge.

Doty, F.D., Entzminger, G., Kulkarni, J., Pamarthy, K. & Staab, J.P., 2007. Radio frequency coil technology for small-animal MRI, *NMR Biomed.,* **20,** 304–325.

Eicken, H., Lensu, M., Leppaeranta, M., Tucker, W.B., III, Gow, A.J. & Salmela, O., 1995. Thickness, structure, and properties of level summer multiyear ice in the Eurasian sector of the Arctic ocean, *J. geophys. Res.,* **100,** 22 697–22 710.

Hand, J.W., 2008. Modelling the interaction of electromagnetic fields (10 MHz-10 GHz) with the human body: methods and applications, *Phys. Med. Biol.,* **53,** R243–R286.

Hertrich, M., 2008. Imaging of groundwater with nuclear magnetic resonance, *Prog. Nucl. Mag. Res. Sp.,* **541,** 227–248.

Hertrich, M., Braun, M., Guenther, T., Green, A.G. & Yaramanci, U., 2007. Surface nuclear magnetic resonance tomography, *IEEE Trans. Geosci. Remote. Sens.,* **45,** 3752–3759.

Hertrich, M., Green, A.G., Braun, M. & Yaramanci, U., 2009. High resolution surface NMR tomography of shallow aquifers based on multi-offset measurements, *Geophysics,* **74** (6), G47–G59.

Hoult, D.I., 2000. The principle of reciprocity in signal strength calculations—a mathematical guide, *Concept Magn. Res.*, **12**(4), 173–187.

Hunter, D. & Kepic, A., 2005. Surface nuclear magnetic resonance signal contribution in conductive terrains, *Expl. Geophys.,* **36,** 73–77.

Jackson, J.D., 2006. *Classical Electrodynamics*, Wiley, New York, NY.

Jin, J., 2002. *The Finite Element Method in Electromagnetics*, Wiley, New York, NY.

Legchenko, A. & Valla, P., 2002. A review of the basic principles for proton magnetic resonance sounding measurements, *J. appl. Geophys.*, **50,** 3–19.

Lehmann-Horn, J.A., Hertrich, M., Greenhalgh, S.A. & Green, A.G., 2011. 3-D magnetic field and NMR sensitivity computation incorporating conductivity anomalies and variable surface topography, *IEEE Trans. Geosci. Remote. Sens.,* **49,** 3878–3891.

Levitt, M.H., 2002. *Spin Dynamics—Basics of Nuclear Magnetic Resonance,* Wiley, Chichester.

McGillivray, P.R. & Oldenburg, D.W., 1990. Methods for calculating Fréchet derivatives and sensitivities for the non-linear inverse problem: a comparative study, *Geophys. Prospect.,* **38,** 499–524.

McGillivray, P.R. & Oldenburg, D.W., 1994. Calculation of sensitivities for the frequency-domain electromagnetic problem, *Geophys. J. Int.,* **116,** 1–4.

Nabighian, M. N., ed., 1992. *Electromagnetic Methods in Applied Geophysics, Vol. II Applications,* Society of Exploration Geophysicists, Tulsa, OK.

Rieben, R., Rodrigue, G. & White, D., 2005. A high order vector finite-element method for solving the time dependent Maxwell equations on unstructured grids, *J. Comput. Phys.,* **204,** 490–519.

Shushakov, O., 1996. Groundwater NMR in conductive water, *Geophysics,* **61**(4), 998–1006.

Suits, B.H., Garroway, A.N. & Miller, J.B., 1998. Surface and gradiometer coils near a conducting body: the lift-off effect, *J. Magn. Reson.,* **135,** 372–379.

Tarantola, A., 2004. *Inverse Problem Theory and Methods for Model Parameter Estimation,* Society for Industrial and Applied Mathematics, Philadelphia, PA.

Walbrecker, J.O., Hertrich, M. & Green, A.G., 2011. Off-resonance effects in surface NMR, *Geophysics,* **76,** 1–12.

Weichman, P.B., Lavely, E.M. & Ritzwoller, M.H., 2000. Theory of surface nuclear magnetic resonance with applications to geophysical imaging problems, *Phys. Rev. E,* **62**(1), 1290–1312.

Wooding, R.A., 1997. Convection in groundwater below an evaporating salt lake: 2. evolution of fingers or plumes, *Water Resour. Res.,* **33,** 1219–1228.

Zhdanov, M.S., 2009. *Geophysical Electromagnetic Theory and Methods*, Elsevier Science & Technology, Oxford.

APPENDIX: SIMPLIFIED SENSITIVITY EXPRESSIONS FOR $B_{1x'} = 0$ AND $B_{1y'} = 0$

In the case of $B_{1x'} = 0$, that is a vanishing x'-component of the complex magnetic field, we can simplify the sensitivity expression using the relations:

$$\hat{\mathcal{B}}_1^{(-)*} = -i\,\hat{B}_{1y'}/2, \tag{A1a}$$

$$\hat{\mathcal{B}}_1^{(+)} = +i\,\hat{B}_{1y'}/2, \tag{A1b}$$

such that eq. (18) becomes:

$$\frac{\partial K}{\partial \sigma} \approx -i\gamma\tau M_0\omega_L I \left\{ \frac{\partial \hat{B}_{1y'}}{\partial \sigma}\hat{B}_{1y'} \right\}. \tag{A2}$$

In the case of $B_{1y'} = 0$, that is a vanishing y'-component of the complex magnetic field, we can simplify the sensitivity expression using:

$$\hat{\mathcal{B}}_1^{(-)*} = \hat{B}_{1x'}/2, \tag{A3a}$$

$$\hat{\mathcal{B}}_1^{(+)} = \hat{B}_{1x'}/2, \tag{A3b}$$

such that eq. (18) becomes:

$$\frac{\partial K}{\partial \sigma} \approx -i\gamma\tau M_0 \omega_L I \left\{ \frac{\partial \hat{B}_{1x'}}{\partial \sigma} \hat{B}_{1x'} \right\}. \tag{A4}$$

In both cases only one of the component x' or y' contributes to the sensitivity functions. In the second case $B_{1y'} = 0$, the sensitivity $\partial K/\partial \sigma$ has the same shape as shown in Figs 5(a) and (b) (at two different spin locations P1 and P2) but scaled by the complex factors given in eq. (A4).